processes

MDPI

Article

Construction of Water Vapor Stable Ultramicroporous Copper-Based Metal–Organic Framework for Efficient CO_2 Capture

Fengfan Yang [1], Xiaolu Wang [1], Jiayue Tian [2], Xusheng Wang [3] and Linfeng Liang [1,*]

[1] Institute of Crystalline Materials, Shanxi University, Taiyuan 030006, China; 202122801030@email.sxu.edu.cn (F.Y.); 201912801009@email.sxu.edu.cn (X.W.)
[2] School of Materials and Chemical Engineering, Zhengzhou University of Light Industry, Zhengzhou 450001, China; jytian@zzuli.edu.cn
[3] School of Materials Science and Engineering, Zhejiang Sci-Tech University, Hangzhou 310018, China; xswang@zstu.edu.cn
* Correspondence: jtcl@sxu.edu.cn; Tel.: +86-351-7016082

Abstract: It is quite essential to obtain an excellent CO_2 adsorption capacity, CO_2 adsorption selectivity and water vapor stability at the same time for practical CO_2 capture after combustion. Through the combination of ultramicropore and the high density of CO_2-philic sites without OMSs, an ultramicroporous Cu-based metal–organic framework has been designed and synthesized, featuring a high CO_2 capacity (99 $cm^3\ g^{-1}$ and 56.6 $cm^3\ g^{-1}$ at 273 K and 298 K, respectively), high selectivity over N_2 (118 at a scale of CO_2/N_2 15/85, 298 K) and excellent water vapor stability, simultaneously. Theoretical calculations indicate that neighboring ketonic O atoms with suitable distance play vital roles in boosting CO_2 selective capture.

Keywords: porous material; MOFs; carbon dioxide; energy; environment

Citation: Yang, F.; Wang, X.; Tian, J.; Wang, X.; Liang, L. Construction of Water Vapor Stable Ultramicroporous Copper-Based Metal–Organic Framework for Efficient CO_2 Capture. *Processes* **2023**, *11*, 1387. https://doi.org/10.3390/pr11051387

Academic Editor: Federica Raganati

Received: 15 March 2023
Revised: 18 April 2023
Accepted: 26 April 2023
Published: 4 May 2023

1. Introduction

With the development of the industry, human demand for energy is increasing, and fossil fuels are still our main source of energy today. This has led to a dramatic increase in greenhouse gas emissions in the atmosphere. The greenhouse effect caused by excessive emissions of greenhouse gases such as CO_2, CH_4, O_3, NO_2 and Freon is the main cause of global warming. Among them, CO_2, as the greenhouse gas with the highest concentration in the atmosphere, produces about 60% of the total greenhouse effect of all greenhouse gases. Over the past few decades, with the dramatic increase in the global population and rapid economic industrialization, energy consumption has also increased dramatically. Although the rapid development of technology has been accompanied by an increasing variety of energy sources, it is estimated that about 60% of global CO_2 emissions come from fossil fuel power generation [1]. In general, there are strategies to reduce CO_2 emissions in the environment through efficient energy use, the use of hydrogen and renewable energy as alternatives to fossil fuels, and the development of new carbon capture technologies. Thus, the installation of effective CO_2 capture systems in coal-fired or gas-fired power plants, which can selectively remove CO_2 in fluid gas, could greatly reduce global CO_2 emissions. The main CO_2 capture technologies currently used are chemisorption and physical adsorption [2]. Industrially, the current mainstream technology is chemisorption using organic amines. Although this technology is capable of absorbing 98% of CO_2 in the exhaust gas, it has disadvantages such as high energy consumption, large amounts of adsorbent and high corrosiveness. Compared with the traditional chemisorption method using organic amines, physical adsorption technology using porous materials exhibits a great prospect due to its facile regeneration process without corrosion problems [3–9].

Zeolite molecular sieves are a class of traditional microporous materials, and their microporous environment with a high density of Lewis polar sites gives these materials considerable CO_2 adsorption capacity and selectivity. For example, according to NaY [10], their CO_2 adsorption capacity can reach 5.5 mmol g^{-1} at 305 K and 1 atm. According to Siriwardane [11], the CO_2 adsorption capacity and selectivity can be maximized by adjusting the specific surface area, metal type and content of the material framework. Unfortunately, zeolite molecular sieves have strong interactions with water molecules and preferentially adsorb water molecules in their presence, which is detrimental to CO_2 capture. Studies have shown that activated carbon has a stronger affinity to CO_2 compared to zeolite while interacting weaker with N_2, thus showing excellent selectivity for CO_2 gas. However, activated carbon is very sensitive to temperature changes, and its CO_2 capture capacity decreases sharply with increasing temperature, while CO_2/N_2 selectivity becomes poor as a result. Du [12] investigated the CO_2 adsorption isotherms of Ajax-activated carbon at three different temperatures at 10 kPa and found that the CO_2 adsorption capacity of this material decreased with increasing temperature. In recent years, a new class of porous material-metal organic frameworks (MOFs), also known as porous coordination polymers (PCPs) and porous coordination networks (PCNs), have been developed into one of the hot spots of research in chemistry and materials. Metal–organic frameworks (MOFs) are considered to be promising materials for CO_2 adsorption compared to inorganic porous materials. The material is an organic–inorganic hybrid material consisting of metal centers (metal ions or metal clusters, SUB) that are self-assembled with organic ligands through coordination bonds to form crystalline porous materials with a periodic network structure. Metal–organic frameworks (MOFs) have attracted a lot of attention as CO_2 capture adsorbents due to their advantages, such as high crystallinity, the precise modularity of their pore size and easy functionality of the pore walls [13–16].

A high CO_2 adsorption capability, CO_2 adsorption selectivity and water vapor stability are very important prerequisites for ideal adsorbents; however, it is not easy to obtain all of these benefits at the same time. For example, various kinds of open metal sites (OMSs) have been widely introduced into the framework as CO_2-philic sites to boost CO_2 capture capability, and this has afforded an exceptionally high CO_2 adsorption capacity and high selectivity for CO_2 in some famous MOFs such as the MOF-74 series [17–31]. However, the activated OMSs could rapidly reabsorb water molecules, thus inevitably resulting in a remarkable decline in CO_2 adsorption capacity in the presence of water vapor, which is commonly seen in fluid gas. Meanwhile, the linkage between the metal junction and the ligand usually becomes fragile with the presence of water vapor, causing concerns about structural stability [32–35]. For another, ligands with polar groups such as hydroxyl, free carboxyl and uncoordinated N atom, etc., have been adopted to build MOFs with saturated coordinated metal ions (that is, no OMSs) to alleviate the negative effects imposed by water vapor, while the CO_2 selectivity of MOFs bearing such functional sites under ambient conditions is usually low because of their relatively weak CO_2–framework interactions [36–40]. According to recent reports, the selectivity of CO_2 can be greatly improved by adjusting the pore size falling in the ultra-microporous range due to CO_2's increased affinity in confined space and the molecular sieving effect [41–43].

Based on the above considerations, the construction of MOF materials with ultra-micropore and the high density of CO_2-philic sites without OMSs has the potential to enhance CO_2 adsorption capacity, improve CO_2 selectivity and strengthen water vapor stability simultaneously. By selecting 5-(1H-1,2,4-triazol-1-yl) isophthalic acid (H_2TIPA) with multiple coordination sites as the organic ligand (Figure 1) and Cu(II) paddle-wheel as the metal node, a new Cu-MOF **SXU−5** was synthesized, and the above goals were satisfied all at once. Although the same ligand was used to synthesize a Cu-MOF, our synthesis conditions were different and led to a crystal structure with a different space group [21]. The significance of using the same ligand to explore new Cu-MOF synthesis lies in the potential to systematically investigate the effect of various reaction conditions on the resulting materials while maintaining a constant ligand framework. By keeping the

ligand constant, the changes in the properties of the resulting MOFs can be attributed to variations in the synthetic parameters, allowing for the identification of structure–property relationships. Therefore, synthesizing new Cu-MOFs with the same linker can identify new MOF candidates with the desired CO_2 adsorption properties and guide subsequent design and synthesis. Owing to the short distance between two different functional groups from the H_2TIPA ligand, the pore size of **SXU−5** falls into the ultramicroporous category (<5–7 Å). As expected, activated **SXU−5** reveals a high CO_2 adsorption quality of 99 cm^3 g^{-1} and 56 cm^3 g^{-1} at 273 K and 298 K, respectively. Its IAST selectivity for CO_2 over N_2 is as high as 118 at a CO_2/N_2 proportion of 15/85 at 298 K, which is comparable to some of the best-performing CO_2 capture materials [44–46]. Theoretical calculations indicate how neighboring two ketonic O atoms with a suitable distance can play a vital role in boosting CO_2 selectively capture.

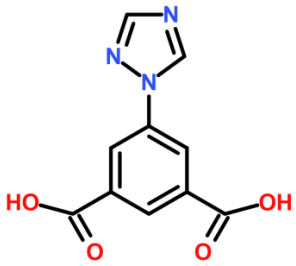

Figure 1. The schematic diagram of the organic ligand H_2TIPA.

2. Materials and Methods

All reagents and solvents were purchased from chemical suppliers without further purification. The ligand H_2TIPA was purchased from Jinan Henghua Co., Ltd. (Shanghai, China) and characterized by ^{1}H NMR experiments (Figure S1). Thermogravimetric analysis (TGA) was carried out on a NETZSCH STA 449C thermal analyzer at a rate of 10 °C/min under a nitrogen (N_2) atmosphere from 30 to 900 °C. At 40 kV and 40 mA, powder X-ray diffraction (PXRD) experiments were performed on a Rigaku Ultima IV X-ray diffractometer with a scanning rate of 1°/min in the 2θ range of 3–40°, and the diffractometer was equipped with a Cu sealed tube (λ = 0.15406 nm). Based on single crystal diffraction data, simulated PXRD patterns were generated by Mercury 3.9 software.

2.1. Synthesis of SXU-5

A mixture of $Cu(NO_3)_2{\cdot}3H_2O$ (0.05 mmol, 12 mg) and H_2TIPA (0.05 mmol, 11.6 mg) was dissolved in H_2O (1 mL), DMF (Dimethyl Formamide, 2 mL) and DMA (Dimethylacetamide, 1 mL) in a 20 mL glass vial. Then, the sealed vial was sonicated for 15 min and heated at 85 °C for 72 h. After cooling naturally to room temperature, blue rod-shaped crystals were obtained after washing with fresh DMA three times (yield, 78%, based on H_2TIPA ligand).

2.2. Gas Adsorption

The Quantachrome instrument and Asiqwin system were used to obtain gas adsorption isotherms. To obtain samples free of guests, approximately 100 mg of fresh **SXU−5** was soaked three times in 20 mL of ethanol for 72 h to exchange high-boiling-point guest molecules in its 1D channels, followed by outgassing under a dynamic vacuum at 100 °C for 8 h. The adsorption isotherm of N_2 was observed in a liquid nitrogen bath at 77 K. Pore size distribution (PSD) data were acquired from N_2 isotherms according to the no-local density functional theory (NLDFT) model (Figure S2). The specific surface area of **SXU−5** was calculated by the BET and Langmuir model from the N_2 adsorption isotherm at 77 K. Room temperature adsorption isotherms of CO_2, N_2, CH_4, C_2H_2, C_2H_4 and C_2H_6 were measured in an ice-water bath (273 K) and water bath (298 K), respectively.

2.3. Thermal Weight Analysis

Thermogravimetric analysis was performed on a NETZSCH STA 449C thermogravimetric analyzer. An appropriate amount of leach extract with mother liquor was taken and extracted and then ramped up from 35 °C to 900 °C at a ramp rate of 10 °C/min under a N_2 atmosphere. The process of change in the material structure can be characterized by temperature.

2.4. Variable Temperature X-ray Powder Diffraction Testing

The structural changes of samples from 30 °C to 300 °C can be tested in a variable temperature X-ray powder diffractometer. The test conditions were as follows: a scanning range of 5–40 °C and a scanning rate of 1°/min. Information on structural changes at different temperatures was characterized.

2.5. Single-Crystal X-ray Diffraction (SC-XRD) Studies

Single-crystal data of **SXU—5** were collected on a Rigaku Oxford single-crystal diffractometer with graphite-monochromated Cu Kα radiation at 77 K. The structure (Table 1) was solved with SHELXT [47], refined by full-matrix least squares on $|F|^2$ by SHELXL,[32] and interfaced through the program OLEX2 [48]. All non-H-atoms were refined anisotropically, and H-atoms were fixed in geometrically estimated positions and refined using the riding model unless stated. Highly disordered solvent molecules were treated with the *SQUEEZE* routine of PLATON [49].

Table 1. Crystallographic data and structural refinement summary.

Compound	SXU-5
CCDC	No. 2012534
Empirical	$C_{10}H_5CuN_3O_4$
Formula weight	294.71
Temperature (K)	100.0(3)
Crystal system	monoclinic
Space group	$P2_1/c$
a (Å)	10.8510(3)
b (Å)	11.7772(3)
c (Å)	14.6364(5)
α (°)	90
β (°)	109.695(3)
γ (°)	90
Volume(Å^3)	1761.03(9)
Z	4
D_c (g cm^{-3})	1.112
μ (mm $^{-1}$)	1.841
F (000)	588
Crystal size (mm^3)	0.2 × 0.1 × 0.1
Radiation	CuKα (λ = 1.54184)
Goodness-of-fit on F^2	1.098
Final R indexes [I ≥ 2σ (I)] [a]	R_1 = 0.0699, wR_2 = 0.2140
Final R indexes [all data] [a]	R_1 = 0.0771, wR_2 = 0.2223
Largest diff. peak/hole/e Å^{-3}	1.74/−1.95

$R_1 = \sum||F_0| - |F_c||/\sum|F_0|$; $wR_2 = [\sum w(|F_0|^2 - |F_c|_2)^2/\sum w(F_0^2)^2]^{1/2}$.

3. Results and Discussion

3.1. Description of Structure

Single-crystal X-ray structure analysis indicates that **SXU—5** crystallizes in the monoclinal space group $P2_1/c$ based on binuclear paddle-wheel Cu secondary building units (SBUs) and $TIPA^{2-}$ organic ligands. As depicted in Figure 1a, each binuclear Cu_2 SBU comprises eight O atoms from four distinct carboxylate groups and two axially located

imine N atoms from two different 1,2,4-triazole groups, representing a distorted octahedral configuration. Each $TIPA^{2-}$ adopts three-coordinated distorted triangle geometry and is coordinated to three different Cu_2 SBUs. The Cu-O and Cu-N bond lengths fall within the normal scope of 2.11(8)–2.398(12) Å and 2.71(2)–2.83(2) Å, respectively [50–52]. There are one-dimensional (1D) rhombic zigzag passages along the crystallographic c-axis (Figure 2b,c) with a pore limiting diameter (PLD) of approx 3.6 Å based on Zeo++_V0.3 software analysis [53], which falls between the dynamic diameters of carbon dioxide (3.4 Å) and nitrogen molecules (3.64 Å), suggesting a strong molecular sieving effect. The total solvent accessible volume for **SXU−5** was approximately 45% based on the *PLATON* calculation using a probe radius of 1.2 Å, indicating its high porosity [49]. Notably, the 1D channels of **SXU−5** were decorated with a high density of uncoordinated N atoms (3.77 mol L^{-1}) [40], which are known for their CO_2-philic characteristics. Topologically, **SXU−5** can be simplified with a Schlafli symbol of $(4.6^2)_2(4^2.6^{10}.8^3)$ (*apo-topology*), as the metal node and organic linker are seen as six- and three-connected nodes, respectively (Figure 2d).

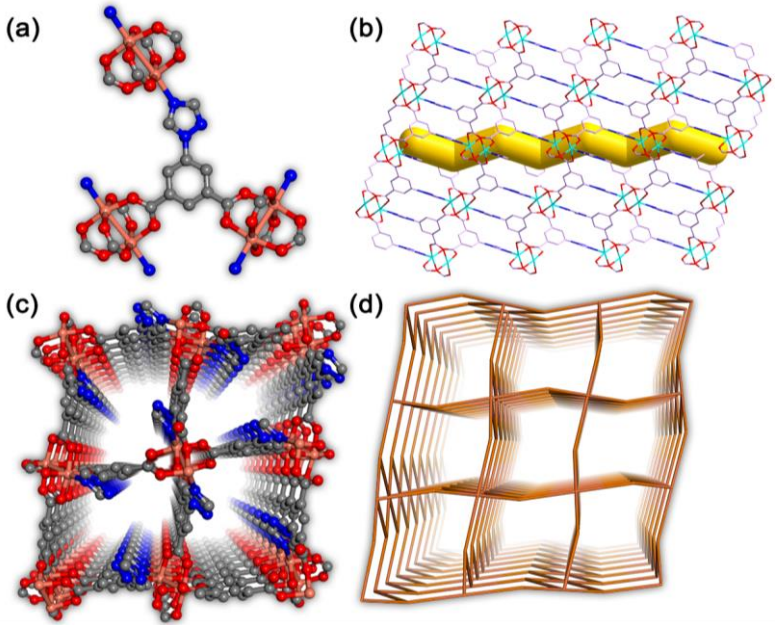

Figure 2. (**a**) The coordination environment of Cu_2 SBUs and organic $TIPA^{2-}$ ligand (Cu atom, coral; C atom, gray; N atom, blue; O atom, red); (**b**) A 3D structure viewed along the b-axis showing the 1D zigzag channel of **SXU−5** (Cu atom, cyan; C atom, purple; other atoms use the same color scale as in ((**a**)); (**c**) the rhombic channels along the a direction with high density of uncoordinated N atoms; (**d**) the simplified framework with Schlafli symbol of $(4.6^2)_2(4^2.6^{10}.8^3)$.

3.2. Stability

The phase purity of as-synthesized **SXU−5** was demonstrated by a powder X-ray diffraction (PXRD) experiment with experimental and simulated patterns in good agreement (Figure 3a). Thermogravimetric analysis (TGA) was first used to evaluate its thermal stability displaying two-step weightlessness (Figure S3). The first step of weightlessness from 25 °C to 270 °C was mainly attributed to the removal of guest molecules in the lattice (calcd 35%). After 300 °C, continual weight loss appeared due to the collapse of the framework and the decomposition of organic ligands. Varied temperature PXRD (VT-PXRD) patterns revealed a good agreement with a simulated pattern, while structural changes appear with the peak around 2θ = 15°, which shifted to higher angles after 150 °C, presumably due to its structural flexibility (Figure 3c). High-temperature SC-XRD or powder pattern Rietveld refinements are good methods to enhance our understanding of structural changes in the sample. Unfortunately, our laboratory does not have the capability to perform high-temperature SC-XRD measurements at these temperatures and also lacks the

expertise to perform Rietveld refinements. The main frame structure maintains stability in the temperature range of 200 °C to 250 °C, implying its good thermal stability. Moreover, the main diffraction peaks of as-synthesized **SXU−5** samples after immersion in different solvents, including diethyl ether, N-propanol, N-hexane and isopropanol for 24 h, matched well with the simulated result except for the lowered diffraction intensities of low-angle peaks around 12/13 degrees, indicating that the X-ray was scattered by the adsorbed molecules (Figure 3a).

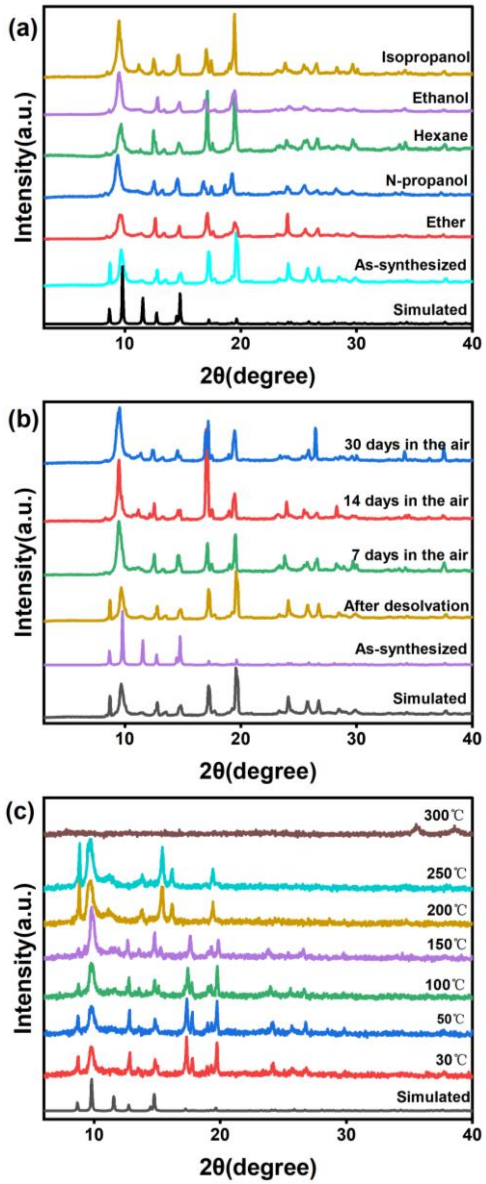

Figure 3. (**a**) PXRD patterns of **SXU−5** after soaking in different solvents for 24 h; (**b**) PXRD patterns off **SXU−5** after exposure to water vapor for 7, 14 and 30 days; (**c**) VT-PXRD patterns of **SXU−5** at different temperatures.

Considering the fact that exhaust gas emissions from coal-fired power plants usually include water vapor (5–7%), adsorbents for the practical post-combustion of CO_2 capture should be steady enough toward water vapor [54–57], and it is necessary to explore the stability of **SXU−5** when subjected to water molecule attacks before the CO_2 adsorption test. After exposure to a laboratory atmosphere at an ambient humidity (about 70%) for 7, 14 and even 30 days, the PXRD peaks exhibited no obvious change, revealing its excellent water vapor stability (Figure 3b) and indicating the potential for capturing CO_2

in the flue gas. Generally, many reported Cu carboxylate MOFs are prone to collapse in the case of water vapor, and just a few well-known MOFs exhibit practical water vapor stability [32,58–60]. The improved water vapor stability of **SXU−5** may be explained from a structural viewpoint in that the coordination sites of binuclear copper are fully occupied by O atoms and N atoms from a 1, 2, 4-triazole moiety with large steric hindrance, which can protect the metal nod from water molecule attacks. We have conducted PXRD tests on the SXU-5 samples before and after immersion in water for 3 h. The PXRD patterns of the water-soaked samples before and after soaking are shown in Figure S4. It can be observed that after immersion, the diffraction peaks of the samples became broader, and their intensity decreased. Furthermore, most of the diffraction peaks did not match those of the as-synthesized sample, indicating that the structure collapsed after direct immersion in water.

3.3. Permanent Porosity

To assess the permanent porosity of **SXU−5**, an activation process was carried out as follows: firstly, about 100 mg of the synthesized **SXU−5** was washed several times with DMF (N,N-dimethylformamide) by ultrasonication and soaked in 20 mL of ethanol for 3 days, exchanging high boiling point guest molecules in its 1D channels. In order to exchange the high boiling point solvent in the frame more thoroughly, we changed the fresh ethanol solvent every 24 h. Then, the solvent exchanged **SXU−5** was outgassed at 100 °C for 8 h to produce desolvated **SXU−5**. This process, called activation, is designed to displace the ligand through a high boiling point solvent in the framework with a low boiling point solvent and then remove the low boiling point solvent from the pore by vacuum drying to achieve a pore that is free of guest molecules. Compared with the as-synthesized sample, the PXRD pattern of desolvated **SXU−5** showed no obvious change, revealing that the structure was preserved after the activation process (Figure 3b). The N_2 adsorption isotherm of desolvated **SXU−5** at 77 K was obtained with typical type-I isotherm characteristics, indicating its microporous nature (Figure 4a). Based on the adsorption data in the low-pressure range, the surface areas of BET and Langmuir were calculated to be 635 $m^2\ g^{-1}$ and 883 $m^2\ g^{-1}$, respectively. The pore volume was estimated to be 0.34 $cm^3\ g^{-1}$ according to the saturation uptake of N_2 (222 $cm^3\ g^{-1}$), which is consistent with the results of single crystal data (0.4 $cm^3\ g^{-1}$), further confirming the sample's good crystallinity and purity.

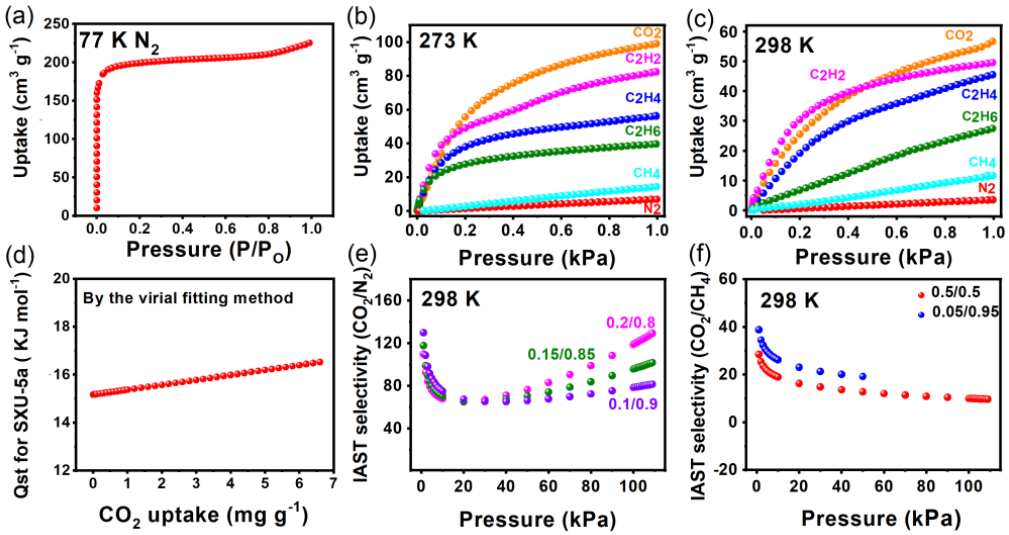

Figure 4. (**a**) N_2 adsorption isotherm of **SXU−5** at 77 K; CO_2, N_2, CH_4, C_2H_4, C_2H_6 and C_2H_2 sorption isotherms of **SXU−5** at (**b**) 273 K and (**c**) 298 K; (**d**) CO_2 isosteric heat of adsorption for **SXU−5**; (**e**) IAST selectivity of **SXU−5** for CO_2/N_2 at 298 K; (**f**) IAST selectivity of **SXU−5** for CO_2/CH_4 at 298 K.

3.4. Gas Adsorption and Separation

With the establishment of permanent porosity, the water vapor stability and high density of non-coordinated N atoms were distributed on the pore surface of **SXU−5**, inspiring us to further discover its application in selective gas adsorption and separation, especially for CO_2. Low-pressure single-component adsorption isotherms of CO_2, N_2, CH_4, C_2H_2, C_2H_4 and C_2H_6 were measured at 273 K and 298 K separately. As shown in Figure 4b,c, **SXU−5** had a maximum CO_2 uptake of 99 (273 K) and 56 $cm^3\ g^{-1}$ (298 K) at 1 bar. Although the maximum adsorption of CO_2 at an ambient condition was lower than those of MOFs with various OMSs, such as the MOF-74 series, it can still compare favorably with many famous MOFs without OMSs, such as MAF-23 (56.1 $cm^3\ g^{-1}$) [45], $Zn(ain)_2$·(DMF) (51.3 $cm^3\ g^{-1}$) [61], IFMC-1 (60.3 cm^3g^{-1}) [62] and IRMOF-74-III-$(CH_2NH_2)_2$ (67.2 cm^3g^{-1}) [36] (for more comparisons, please see Table S1). This saturation uptake is an important indicator of adsorbents, and further experiments were performed to investigate their selective gas adsorption properties.

The affinity toward guest gas molecules can be indicated by the heat of adsorption (Qst), which was computed from experimental isotherms (calculation details please refer to supporting information) [63]. On the basis of the adsorption isotherms at 273 K and 298 K (Figure S5), the calculated Qst of **SXU−5** toward CO_2 was significantly increased from 15 kJ mol^{-1} to 43.6 kJ mol^{-1} with CO_2 uptake increasing from 0 to 111 mg g^{-1} (Figure 4d). This growing trend indicates that gradually increasing strong CO_2–CO_2 interactions occur inside the narrow pores, which has been observed in previously reported ultra-microporous MOF materials [64–67]. By contrast, the maximum uptakes of N_2 are 6.88 $cm^3\ g^{-1}$ and 3.5 $cm^3\ g^{-1}$ at 273 K and 298 K, separately, which are much less than those of CO_2, revealing their distinct selectivity above N_2. The ideal absorbed solution theory (IAST) was then adopted to compute the absorption selectivity of CO_2/N_2 under different temperatures [68]. Surprisingly, the selectivity for CO_2/N_2 (0.15/0.85) at 1 atm and 298 K was as high as 118 (Figure 4e), which is higher than many famous MOFs with excellent CO_2/N_2 selectivity under the same conditions, such as Co-MOF-74 (25) [69], BUT-11 (31.5) [70], and ZIF-69 (20) [71], indicating the bright prospect of **SXU−5** for practical CO_2 capture and separation. Meanwhile, the IAST selectivity of SXU-5 (CO_2/N_2, 0.15/0.85) at 273 K was as high as 67 (Figure S6). Simulated results from different proportions of CO_2 and N_2 exhibited similar trends at 298 K and 273 K (Figure 4e, Figures S7 and S8), showing a high selectivity toward CO_2 in a wide range. It is worth mentioning that the selectivity was further increased to a higher value of 129 at 298 K when the CO_2/N_2 proportion increased to 0.2/0.8. The above results confirm the considerable application potential of **SXU−5** in practical CO_2 capture, for which the concentration of CO_2 in the wasting gas tends to fluctuate around a certain concentration proportion of 15%.

Apart from the CO_2 capture of the post-combustion fluid, the purification of natural gas, which is mainly composed of methane for high-efficiency utilization, is essential as impurities such as CO_2, C_2H_6, C_2H_4, C_2H_2, etc., greatly reduce its quality [72–74]. **SXU−5** exhibits a very limited uptake towards CH_4, which is considerably lower than the corresponding uptakes of commonly seen natural gas impurities at 273 K and 298 K (Figure 4b,c). As shown in Figure 4c, **SXU−5** displays gradient uptakes for CO_2 (56 $cm^3\ g^{-1}$), C_2H_2 (49.5 $cm^3\ g^{-1}$), C_2H_4 (45.5 $cm^3\ g^{-1}$), C_2H_6 (27.44 $cm^3\ g^{-1}$) and CH_4 (11.6 $cm^3\ g^{-1}$), implying that **SXU−5** can be a promising adsorbent candidate for natural gas decontamination. Taking CO_2 and C_2H_2 as impurities, for example, the predicted IAST selectivity for equimolar CO_2/CH_4 and C_2H_2/CH_4 as a feature of pressure is presented in Figure 4f. With increased pressure, both the CO_2/CH_4 and C_2H_2/CH_4 selectivities decrease in the low-pressure region and then gradually reach stabilization in the range of 36.1–11.5 and 28.5–9.7 at 298 K, respectively. IAST C_2H_2/CH_4 selectivity lies in the upper class compared with those of reported MOFs [75–78]. More importantly, **SXU−5** can selectively adsorb a variety of commonly seen natural gas impurities at the same time, which is very important when simplifying the purification facility, indicating its huge potential in natural gas purification.

To understand the interaction between CO_2 frameworks and selectivity for carbon adsorption for **SXU−5**, we performed grand canonical Monte Carlo (GCMC) in Materials

Studio 8.0 using their crystallographic data as initial models. Compared with the Cu-MOF reported earlier, the research on **SXU−5** focused more on the CO_2 capture mechanism on a molecular level. As shown in Figure 5a, one CO_2 molecule was preferentially adsorbed between two neighboring ketonic atoms in **SXU−5** with O–O distances of 2.85 Å and 2.89 Å at low pressure. Interestingly, different from the extensively accepted viewpoint that uncoordinated N atoms could bind the CO_2 preferentially, our calculation results indicate that two adjacent ketonic O atoms exhibit a stronger affinity with CO_2 molecules. This phenomenon might be due to the weak basic nature of the ketonic O atoms [79,80], exhibiting an affinity for acidic oxides such as CO_2 and their suitable distance, which could corporately contribute to enhancing MOF–CO_2 interactions. In addition, the snapshots for CO_2 adsorption in **SXU−5** at different pressures (Figure 5b–d) clearly indicate that CO_2 molecules were first adsorbed around ketonic atoms in the pores. Once the ketonic O atoms were fully occupied, the CO_2 molecules could fill up the 1D channel with C-O distance from different CO_2 molecules that were smaller than the sum of their Van der Waals radius (Figure S9), contributing to increased Qst values for the enhanced CO_2–CO_2 interactions. Therefore, the excellent selectivity of CO_2 adsorption for **SXU−5** could be due to the fact that the ketonic O atoms have the suitable distance to provide enhanced CO_2 binding interactions.

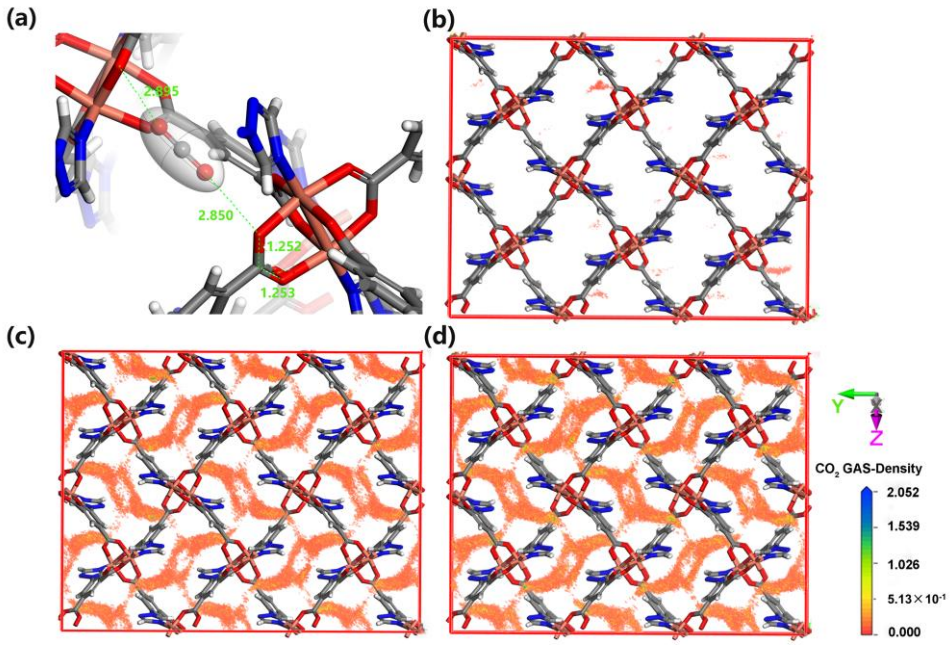

Figure 5. (**a**) The simulated preferential CO_2 adsorption site of **SXU−5** at 298 K (Cu atom, coral; C atom, gray; N atom, blue; O atom, red); (**b**–**d**) are the simulated CO_2 density distribution maps of **SXU−5** at 10, 30, 60 kPa at 298 K, respectively.

4. Conclusions

In conclusion, through the combination of ultramicropore and the high density of CO_2-philic sites without OMSs, we successfully constructed a new ultra-microporous Cu-MOF exhibiting good water vapor stability, high CO_2 uptake capacity (99 cm^3 g^{-1} and 56.6 cm^3 g^{-1} at 273 K and 298 K, respectively) and high selectivity over N_2 (118 at a scale of CO_2/N_2 15/85, 298 K) simultaneously. More importantly, this work demonstrates that two neighboring ketonic O atoms with a suitable distance play vital roles in boosting CO_2 selectively capture and can be referenced for the future design of CO_2 capture materials.

Supplementary Materials: The following supporting information can be downloaded at: https://www.mdpi.com/article/10.3390/pr11051387/s1, Figure S1: The ^{1}H NMR of H_2TIPA ligand; Table S1: Table of the CO_2 uptake capacity of MOFs with literature report.

Author Contributions: F.Y. is responsible for the processing of experimental data and writing the paper, X.W. (Xiaolu Wang) is responsible for conducting synthetic experiments, J.T. and X.W. (Xusheng Wang) are responsible for theoretical simulations, and L.L. is responsible for designing the experiments and modifying the paper. All authors have read and agreed to the published version of the manuscript.

Funding: This research was funded by the National Natural Science Foundation of China (22001154).

Data Availability Statement: Not applicable.

Acknowledgments: We would like to thank Daqiang Yuan from the Fujian Institute of Research on the Structure of Matter for his assistance in single crystal data processing.

Conflicts of Interest: The authors declare no conflict of interest.

References

1. Metz, B.; Davidson, O.R.; Bosch, P.R.; Dave, R.; Meyer, L.A. *Contribution of Working Group III to the Fourth Assessment Report of the Intergovernmental Panel on Climate Change*; Cambridge University Press: Cambridge, UK, 2007; pp. 27–93.
2. Hepburn, C.; Adlen, E.; Beddington, J.; Carter, E.A.; Fuss, S.; Mac Dowell, N.; Minx, J.C.; Smith, P.; Williams, C.K. The technological and economic prospects for CO_2 utilization and removal. *Nature* **2019**, *575*, 87–97. [CrossRef] [PubMed]
3. Xie, Y.; Wang, T.-T.; Liu, X.-H.; Zou, K.; Deng, W.-Q. Capture and conversion of CO_2 at ambient conditions by a conjugated microporous polymer. *Nat. Commun.* **2013**, *4*, 1960. [CrossRef]
4. Li, Y.; Li, L.; Yu, J. Applications of Zeolites in Sustainable Chemistry. *Chem* **2017**, *3*, 928–949. [CrossRef]
5. Feng, X.; Ding, X.; Jiang, D. Covalent organic frameworks. *Chem. Soc. Rev.* **2012**, *41*, 6010–6022. [CrossRef] [PubMed]
6. Trickett, C.A.; Helal, A.; Al-Maythalony, B.A.; Yamani, Z.H.; Cordova, K.E.; Yaghi, O.M. The chemistry of metal–organic frameworks for CO_2 capture, regeneration and conversion. *Nat. Rev. Mater.* **2017**, *2*, 17045. [CrossRef]
7. Lin, R.-B.; He, Y.; Li, P.; Wang, H.; Zhou, W.; Chen, B. Multifunctional porous hydrogen-bonded organic framework materials. *Chem. Soc. Rev.* **2019**, *48*, 1362–1389. [CrossRef]
8. Puthiaraj, P.; Lee, Y.-R.; Ahn, W.-S. Microporous amine-functionalized aromatic polymers and their carbonized products for CO2 adsorption. *Chem. Eng. J.* **2017**, *319*, 65–74. [CrossRef]
9. D'Alessandro, D.M.; Smit, B.; Long, J.R. Carbon Dioxide Capture: Prospects for New Materials. *Angew. Chem. Int. Ed.* **2010**, *49*, 6058–6082. [CrossRef]
10. Dunne, J.A.; Mariwala, R.; Rao, M.; Sircar, S.; Gorte, R.J.; Myers, A.L. Calorimetric Heats of Adsorption and Adsorption Isotherms. 1. O_2, N_2, Ar, CO_2, CH_4, C_2H_6, and SF_6 on Silicalite. *Langmuir* **1996**, *12*, 5888–5895. [CrossRef]
11. Siriwardane, R.V.; Shen, M.-S.; Fisher, E.P. Adsorption of CO_2, N_2, and O_2 on natural zeolites. *Energy Fuels* **2003**, *17*, 571–576. [CrossRef]
12. Do, D.; Wang, K. A new model for the description of adsorption kinetics in heterogeneous activated carbon. *Carbon* **1998**, *36*, 1539–1554. [CrossRef]
13. Li, J.-R.; Kuppler, R.J.; Zhou, H.-C. Selective gas adsorption and separation in metal–organic frameworks. *Chem. Soc. Rev.* **2009**, *38*, 1477–1504. [CrossRef]
14. Zhang, Z.; Yao, Z.-Z.; Xiang, S.; Chen, B. Perspective of microporous metal–organic frameworks for CO_2 capture and separation. *Energy Environ. Sci.* **2014**, *7*, 2868–2899. [CrossRef]
15. Furukawa, H.; Cordova, K.E.; O'Keeffe, M.; Yaghi, O.M. The Chemistry and Applications of Metal-Organic Frameworks. *Science* **2013**, *341*, 1230444. [CrossRef]
16. Ding, M.; Flaig, R.W.; Jiang, H.-L.; Yaghi, O.M. Carbon capture and conversion using metal–organic frameworks and MOF-based materials. *Chem. Soc. Rev.* **2019**, *48*, 2783–2828. [CrossRef]
17. Caskey, S.R.; Wong-Foy, A.G.; Matzger, A.J. Dramatic tuning of carbon dioxide uptake via metal substitution in a coordination polymer with cylindrical pores. *J. Am. Chem. Soc.* **2008**, *130*, 10870–10871. [CrossRef]
18. Li, Y.-W.; Li, J.-R.; Wang, L.-F.; Zhou, B.-Y.; Chen, Q.; Bu, X.-H. Microporous metal–organic frameworks with open metal sites as sorbents for selective gas adsorption and fluorescence sensors for metal ions. *J. Mater. Chem. A* **2012**, *1*, 495–499. [CrossRef]
19. Tan, Y.-X.; He, Y.-P.; Zhang, J. Pore partition effect on gas sorption properties of an anionic metal–organic framework with exposed Cu^{2+} coordination sites. *Chem. Commun.* **2011**, *47*, 10647–10649. [CrossRef]
20. McDonald, T.M.; Lee, W.R.; Mason, J.A.; Wiers, B.M.; Hong, C.S.; Long, J.R. Capture of carbon dioxide from air and flue gas in the alkylamine-appended metal–organic framework mmen-Mg2 (dobpdc). *J. Am. Chem. Soc.* **2012**, *134*, 7056–7065. [CrossRef]
21. Ma, Z.L.; Liu, P.X.; Liu, Z.Y.; Wang, J.J.; Li, L.B.; Tian, L. A thermally and chemically stable copper (II) metal–organic framework with high performance for gas adsorption and separation. *Inorg. Chem.* **2021**, *60*, 6550–6558. [CrossRef]
22. Lin, R.-B.; Li, L.; Wu, H.; Arman, H.; Li, B.; Lin, R.-G.; Zhou, W.; Chen, B. Optimized separation of acetylene from carbon dioxide and ethylene in a microporous material. *J. Am. Chem. Soc.* **2017**, *139*, 8022–8028. [CrossRef]
23. Liu, X.; Xiao, Z.; Xu, J.; Xu, W.; Sang, P.; Zhao, L.; Zhu, H.; Sun, D.; Guo, W. A NbO-type copper metal–organic framework decorated with carboxylate groups exhibiting highly selective CO_2 adsorption and separation of organic dyes. *J. Mater. Chem. A* **2016**, *4*, 13844–13851. [CrossRef]

24. Zheng, B.; Liu, H.; Wang, Z.; Yu, X.; Yia, P.; Bai, J. Porous NbO-type metal–organic framework with inserted acylamide groups exhibiting highly selective CO_2 capture. *CrystEngComm* **2013**, *15*, 3517–3520. [CrossRef]
25. Shi, Y.; Xie, Y.; Cui, H.; Alothman, Z.A.; Alduhaish, O.; Lin, R.-B.; Chen, B. An ultramicroporous metal–organic framework with dual functionalities for high sieving separation of CO2 from CH4 and N2. *Chem. Eng. J.* **2022**, *446*, 137101. [CrossRef]
26. Du, Y.; Chen, Y.; Wang, Y.; He, C.; Yang, J.; Li, L.; Li, J. Optimized pore environment for efficient high selective C_2H_2/C_2H_4 and C_2H_2/CO_2 separation in a metal-organic framework. *Sep. Purif. Technol.* **2021**, *256*, 117749. [CrossRef]
27. Lee, J.; Chuah, C.Y.; Kim, J.; Kim, Y.; Ko, N.; Seo, Y.; Kim, K.; Bae, T.H.; Lee, E. Separation of Acetylene from Carbon Dioxide and Ethylene by a Water-Stable Microporous Metal-Organic Framework with Aligned Imidazolium Groups inside the Channels. *Angew. Chem.* **2018**, *130*, 7995–7999. [CrossRef]
28. Luo, F.; Yan, C.; Dang, L.; Krishna, R.; Zhou, W.; Wu, H.; Dong, X.; Han, Y.; Hu, T.-L.; O'keeffe, M.; et al. UTSA-74: A MOF-74 Isomer with Two Accessible Binding Sites per Metal Center for Highly Selective Gas Separation. *J. Am. Chem. Soc.* **2016**, *138*, 5678–5684. [CrossRef]
29. Zhang, Y.; Yang, L.; Wang, L.; Duttwyler, S.; Xing, H. A Microporous Metal-Organic Framework Supramolecularly Assembled from a CuII Dodecaborate Cluster Complex for Selective Gas Separation. *Angew. Chem.* **2019**, *131*, 8229–8234. [CrossRef]
30. Peng, Y.-L.; Pham, T.; Li, P.; Wang, T.; Chen, Y.; Chen, K.; Forrest, K.A.; Space, B.; Cheng, P.; Zaworotko, M.J.; et al. Robust Ultramicroporous Metal-Organic Frameworks with Benchmark Affinity for Acetylene. *Angew. Chem. Int. Ed.* **2018**, *57*, 10971–10975. [CrossRef]
31. Evans, H.A.; Mullangi, D.; Deng, Z.; Wang, Y.; Peh, S.B.; Wei, F.; Wang, J.; Brown, C.M.; Zhao, D.; Canepa, P.; et al. Aluminum formate, Al (HCOO) 3: An earth-abundant, scalable, and highly selective material for CO_2 capture. *Sci. Adv.* **2022**, *8*, eade1473. [CrossRef]
32. Yuan, S.; Feng, L.; Wang, K.; Pang, J.; Bosch, M.; Lollar, C.; Sun, Y.; Qin, J.; Yang, X.; Zhang, P.; et al. Stable metal–organic frameworks: Design, synthesis, and applications. *Adv. Mater.* **2018**, *30*, e1704303. [CrossRef] [PubMed]
33. Furukawa, H.; Gándara, F.; Zhang, Y.-B.; Jiang, J.; Queen, W.L.; Hudson, M.R.; Yaghi, O.M. Water Adsorption in Porous Metal–Organic Frameworks and Related Materials. *J. Am. Chem. Soc.* **2014**, *136*, 4369–4381. [CrossRef]
34. Low, J.J.; Benin, A.I.; Jakubczak, P.; Abrahamian, J.F.; Faheem, S.A.; Willis, R.R. Virtual High Throughput Screening Confirmed Experimentally: Porous Coordination Polymer Hydration. *J. Am. Chem. Soc.* **2009**, *131*, 15834–15842. [CrossRef]
35. Tranchemontagne, D.J.; Mendoza-Cortés, J.L.; O'Keeffea, M.; Yaghi, O.M. Secondary building units, nets and bonding in the chemistry of metal–organic frameworks. *Chem. Soc. Rev.* **2009**, *38*, 1257–1283. [CrossRef]
36. Flaig, R.W.; Popp, T.M.O.; Fracaroli, A.M.; Kapustin, E.A.; Kalmutzki, M.J.; Altamimi, R.M.; Fathieh, F.; Reimer, J.A.; Yaghi, O.M. The Chemistry of CO_2 Capture in an Amine-Functionalized Metal–Organic Framework under Dry and Humid Conditions. *J. Am. Chem. Soc.* **2017**, *139*, 12125–12128. [CrossRef]
37. Li, B.; Zhang, Z.; Li, Y.; Yao, K.; Zhu, Y.; Deng, Z.; Yang, F.; Zhou, X.; Li, G.; Wu, H.; et al. Enhanced binding affinity, remarkable selectivity, and high capacity of CO2 by dual functionalization of a rht-type metal–organic framework. *Angew. Chem. Int. Ed.* **2012**, *51*, 1412–1415. [CrossRef]
38. Fracaroli, A.M.; Furukawa, H.; Suzuki, M.; Dodd, M.; Okajima, S.; Gándara, F.; Reimer, J.A.; Yaghi, O.M. Metal–Organic Frameworks with Precisely Designed Interior for Carbon Dioxide Capture in the Presence of Water. *J. Am. Chem. Soc.* **2014**, *136*, 8863–8866. [CrossRef] [PubMed]
39. Smaldone, R.A.; Forgan, R.; Furukawa, H.; Gassensmith, J.J.; Slawin, A.M.Z.; Yaghi, O.M.; Stoddart, J.F. Metal-Organic Frameworks from Edible Natural Products. *Angew. Chem. Int. Ed.* **2010**, *49*, 8630–8634. [CrossRef] [PubMed]
40. Liao, P.-Q.; Chen, H.; Zhou, D.-D.; Liu, S.-Y.; He, C.-T.; Rui, Z.; Ji, H.; Zhang, J.-P.; Chen, X.-M. Monodentate hydroxide as a super strong yet reversible active site for CO_2capture from high-humidity flue gas. *Energy Environ. Sci.* **2015**, *8*, 1011–1016. [CrossRef]
41. Bao, S.-J.; Krishna, R.; He, Y.-B.; Qin, J.-S.; Su, Z.-M.; Li, S.-L.; Xie, W.; Du, D.-Y.; He, W.-W.; Zhang, S.-R.; et al. A stable metal–organic framework with suitable pore sizes and rich uncoordinated nitrogen atoms on the internal surface of micropores for highly efficient CO_2 capture. *J. Mater. Chem. A* **2015**, *3*, 7361–7367. [CrossRef]
42. Chen, K.-J.; Madden, D.G.; Pham, T.; Forrest, K.A.; Kumar, A.; Yang, Q.-Y.; Xue, W.; Space, B.; Perry, J.J., 4th; Zhang, J.-P.; et al. Tuning Pore Size in Square-Lattice Coordination Networks for Size-Selective Sieving of CO2. *Angew. Chem. Int. Ed. Engl.* **2016**, *55*, 10268–10272. [CrossRef] [PubMed]
43. Han, L.; Pham, T.; Zhuo, M.; Forrest, K.A.; Suepaul, S.; Space, B.; Zaworotko, M.J.; Shi, W.; Chen, Y.; Cheng, P.; et al. Molecular Sieving and Direct Visualization of CO_2 in Binding Pockets of an Ultramicroporous Lanthanide Metal–Organic Framework Platform. *ACS Appl. Mater. Interfaces* **2019**, *11*, 23192–23197. [CrossRef] [PubMed]
44. Kim, S.-N.; Kim, J.; Kim, H.-Y.; Cho, H.-Y.; Ahn, W.-S. Adsorption/catalytic properties of MIL-125 and NH2-MIL-125. *Catal. Today* **2013**, *204*, 85–93. [CrossRef]
45. Liao, P.-Q.; Zhou, D.-D.; Zhu, A.-X.; Jiang, L.; Lin, R.-B.; Zhang, J.-P.; Chen, X.-M. Strong and Dynamic CO_2 Sorption in a Flexible Porous Framework Possessing Guest Chelating Claws. *J. Am. Chem. Soc.* **2012**, *134*, 17380–17383. [CrossRef]
46. Chen, S.; Zhang, J.; Wu, T.; Feng, P.; Bu, X. Multiroute Synthesis of Porous Anionic Frameworks and Size-Tunable Extraframework Organic Cation-Controlled Gas Sorption Properties. *J. Am. Chem. Soc.* **2009**, *131*, 16027–16029. [CrossRef] [PubMed]
47. Sheldrick, G.M. Crystal structure refinement with SHELXL. *Acta Crystallogr. Sect. C Struct. Chem.* **2015**, *71*, 3–8. [CrossRef] [PubMed]

48. Bourhis, L.J.; Dolomanov, O.V.; Gildea, R.J.; Howard, J.A.K.; Puschmann, H. The anatomy of a comprehensive constrained, restrained refinement program for the modern computing environment–Olex2 dissected. *Acta Crystallogr. Sect. A Found. Adv.* **2015**, *71*, 59–75. [CrossRef]
49. Spek, A.L. PLATON SQUEEZE: A tool for the calculation of the disordered solvent contribution to the calculated structure factors. *Acta Crystallogr. Sect. C Struct. Chem.* **2015**, *71*, 9–18. [CrossRef]
50. Xiang, S.; Huang, J.; Li, L.; Zhang, J.; Jiang, L.; Kuang, X.; Su, C.-Y. Nanotubular Metal−Organic Frameworks with High Porosity Based on T-Shaped Pyridyl Dicarboxylate Ligands. *Inorg. Chem.* **2011**, *50*, 1743–1748. [CrossRef]
51. Du, L.; Lu, Z.; Zheng, K.; Wang, J.; Zheng, X.; Pan, Y.; You, X.; Bai, J. Fine-Tuning Pore Size by Shifting Coordination Sites of Ligands and Surface Polarization of Metal–Organic Frameworks To Sharply Enhance the Selectivity for CO_2. *J. Am. Chem. Soc.* **2012**, *135*, 562–565. [CrossRef]
52. Jiang, Z.; Zou, Y.; Xu, T.; Fan, L.; Zhou, P.; He, Y. A hydrostable cage-based MOF with open metal sites and Lewis basic sites immobilized in the pore surface for efficient separation and purification of natural gas and C_2H_2. *Dalton Trans.* **2020**, *49*, 3553–3561. [CrossRef] [PubMed]
53. Willems, T.F.; Rycroft, C.H.; Kazi, M.; Meza, J.C.; Haranczyk, M. Algorithms and tools for high-throughput geometry-based analysis of crystalline porous materials. *Microporous Mesoporous Mater.* **2012**, *149*, 134–141. [CrossRef]
54. Mason, J.A.; McDonald, T.M.; Bae, T.-H.; Bachman, J.E.; Sumida, K.; Dutton, J.J.; Kaye, S.S.; Long, J.R. Application of a high-throughput analyzer in evaluating solid adsorbents for post-combustion carbon capture via multicomponent adsorption of CO_2, N_2, and H_2O. *J. Am. Chem. Soc.* **2015**, *137*, 4787–4803. [CrossRef] [PubMed]
55. Zhang, Z.; Zhao, Y.; Gong, Q.; Li, Z.; Li, J. MOFs for CO_2capture and separation from flue gas mixtures: The effect of multifunctional sites on their adsorption capacity and selectivity. *Chem. Commun.* **2012**, *49*, 653–661. [CrossRef]
56. Del Grosso, S.J.; Parton, W.J.; Mosier, A.R.; Walsh, M.K.; Ojima, D.S.; Thornton, P.E. DAYCENT National-Scale Simulations of Nitrous Oxide Emissions from Cropped Soils in the United States. *J. Environ. Qual.* **2006**, *35*, 1451–1460. [CrossRef] [PubMed]
57. Heath, L.S.; Smith, J.E.; Skog, K.E.; Nowak, D.J.; Woodall, C.W. Managed Forest carbon estimates for the US greenhouse gas inventory, 1990—2008. *J. For.* **2011**, *109*, 167–173.
58. Wang, B.; Lv, X.-L.; Feng, D.; Xie, L.-H.; Zhang, J.; Li, M.; Xie, Y.; Li, J.-R.; Zhou, H.-C. Highly stable Zr (IV)-based metal–organic frameworks for the detection and removal of antibiotics and organic explosives in water. *J. Am. Chem. Soc.* **2016**, *138*, 6204–6216. [CrossRef]
59. Bai, Y.; Dou, Y.; Xie, L.-H.; Rutledge, W.; Li, J.-R.; Zhou, H.-C. Zr-based metal–organic frameworks: Design, synthesis, structure, and applications. *Chem. Soc. Rev.* **2016**, *45*, 2327–2367. [CrossRef]
60. Lv, X.-L.; Wang, K.; Wang, B.; Su, J.; Zou, X.; Xie, Y.; Li, J.-R.; Zhou, H.-C. A base-resistant metalloporphyrin metal–organic framework for C–H bond halogenation. *J. Am. Chem. Soc.* **2017**, *139*, 211–217. [CrossRef]
61. Wang, F.; Tan, Y.-X.; Yang, H.; Kang, Y.; Zhang, J. Open diamondoid amino-functionalized MOFs for CO_2 capture. *Chem. Commun.* **2012**, *48*, 4842–4844. [CrossRef]
62. Qin, J.-S.; Du, D.-Y.; Li, W.-L.; Zhang, J.-P.; Li, S.-L.; Su, Z.-M.; Wang, X.-L.; Xu, Q.; Shaoa, K.-Z.; Lan, Y.-Q. N-rich zeolite-like metal–organic framework with sodalite topology: High CO_2 uptake, selective gas adsorption and efficient drug delivery. *Chem. Sci.* **2012**, *3*, 2114–2118. [CrossRef]
63. Rowsell, J.L.; Yaghi, O.M. Effects of functionalization, catenation, and variation of the metal oxide and organic linking units on the low-pressure hydrogen adsorption properties of metal−organic frameworks. *J. Am. Chem. Soc.* **2006**, *128*, 1304–1315. [CrossRef] [PubMed]
64. Nugent, P.S.; Rhodus, V.L.; Pham, T.; Forrest, K.; Wojtas, L.; Space, B.; Zaworotko, M.J. A Robust Molecular Porous Material with High CO_2 Uptake and Selectivity. *J. Am. Chem. Soc.* **2013**, *135*, 10950–10953. [CrossRef]
65. Wang, H.; Li, B.; Wu, H.; Hu, T.-L.; Yao, Z.; Zhou, W.; Xiang, S.; Chen, B. A Flexible Microporous Hydrogen-Bonded Organic Framework for Gas Sorption and Separation. *J. Am. Chem. Soc.* **2015**, *137*, 9963–9970. [CrossRef] [PubMed]
66. Xiang, S.; He, Y.; Zhang, Z.; Wu, H.; Zhou, W.; Krishna, R.; Chen, B. Microporous metal-organic framework with potential for carbon dioxide capture at ambient conditions. *Nat. Commun.* **2012**, *3*, 954. [CrossRef]
67. Zhao, X.; Bu, X.; Nguyen, E.T.; Zhai, Q.-G.; Mao, C.; Feng, P. Multivariable Modular Design of Pore Space Partition. *J. Am. Chem. Soc.* **2016**, *138*, 15102–15105. [CrossRef]
68. Myers, A.L.; Prausnitz, J.M. Thermodynamics of mixed-gas adsorption. *AIChE J.* **1965**, *11*, 121–127. [CrossRef]
69. Cho, H.-Y.; Yang, D.-A.; Kim, J.; Jeong, S.-Y.; Ahn, W.-S. CO2 adsorption and catalytic application of Co-MOF-74 synthesized by microwave heating. *Catal. Today* **2012**, *185*, 35–40. [CrossRef]
70. Wang, B.; Huang, H.; Lv, X.-L.; Xie, Y.; Li, M.; Li, J.-R. Tuning CO_2 selective adsorption over N_2 and CH_4 in UiO-67 analogues through ligand functionalization. *Inorg. Chem.* **2014**, *53*, 9254–9259. [CrossRef]
71. Banerjee, R.; Furukawa, H.; Britt, D.; Knobler, C.; O'keeffe, M.; Yaghi, O.M. Control of Pore Size and Functionality in Isoreticular Zeolitic Imidazolate Frameworks and their Carbon Dioxide Selective Capture Properties. *J. Am. Chem. Soc.* **2009**, *131*, 3875–3877. [CrossRef]
72. Duan, J.; Jin, W.; Krishna, R. Natural Gas Purification Using a Porous Coordination Polymer with Water and Chemical Stability. *Inorg. Chem.* **2015**, *54*, 4279–4284. [CrossRef] [PubMed]
73. He, Y.; Xiang, S.; Zhang, Z.; Xiong, S.; Fronczek, F.R.; Krishna, R.; O'Keeffe, M.; Chen, B. A microporous lanthanide-tricarboxylate framework with the potential for purification of natural gas. *Chem. Commun.* **2012**, *48*, 10856–10858. [CrossRef] [PubMed]

74. He, Y.; Zhou, W.; Krishna, R.; Chen, B. Microporous metal–organic frameworks for storage and separation of small hydrocarbons. *Chem. Commun.* **2012**, *48*, 11813–11831. [CrossRef] [PubMed]
75. Xue, Y.-Y.; Zhang, J.-W.; Li, Y.-P.; Li, H.-P.; Wang, Y.; Li, S.-N.; Jiang, Y.-C.; Hu, M.-C.; Zhai, Q.-G. Mimic of Ferroalloy To Develop a Bifunctional Fe–Organic Framework Platform for Enhanced Gas Sorption and Efficient Oxygen Evolution Electrocatalysis. *ACS Appl. Mater. Interfaces* **2019**, *12*, 4432–4442. [CrossRef]
76. Lysova, A.A.; Samsonenko, D.G.; Dorovatovskii, P.V.; Lazarenko, V.A.; Khrustalev, V.N.; Kovalenko, K.A.; Dybtsev, D.N.; Fedin, V.P. Tuning the Molecular and Cationic Affinity in a Series of Multifunctional Metal–Organic Frameworks Based on Dodecanuclear Zn(II) Carboxylate Wheels. *J. Am. Chem. Soc.* **2019**, *141*, 17260–17269. [CrossRef]
77. Chen, D.-M.; Tian, J.-Y.; Liu, C.-S.; Du, M. A Co^{II}-based metal–organic framework based on $[Co_6(\mu_3\text{-}OH)_4]$ units exhibiting selective sorption of C_2 H_2 over CO_2 and CH_4. *CrystEngComm* **2016**, *18*, 3760–3763. [CrossRef]
78. Ling, Y.; Jiao, J.; Zhang, M.; Liu, H.; Bai, D.; Feng, Y.; He, Y. A porous lanthanide metal–organic framework based on a flexible cyclotriphosphazene-functionalized hexacarboxylate exhibiting selective gas adsorption. *Crystengcomm* **2016**, *18*, 6254–6261. [CrossRef]
79. Li, Y.-Z.; Wang, H.-H.; Yang, H.-Y.; Hou, L.; Wang, Y.-Y.; Zhu, Z. An Uncommon Carboxyl-Decorated Metal-Organic Framework with Selective Gas Adsorption and Catalytic Conversion of CO_2. *Chem. A Eur. J.* **2017**, *24*, 865–871. [CrossRef]
80. Liu, J.; Yang, G.-P.; Jin, J.; Wu, D.; Ma, L.-F.; Wang, Y.-Y. A first new porous d–p HMOF material with multiple active sites for excellent CO_2 capture and catalysis. *Chem. Commun.* **2020**, *56*, 2395–2398. [CrossRef]